



1 **Dynamic response and breakage of trees subject to a landslide-induced air blast:**

2 **Implications for air blasts risk assessment in mountainous regions**

3 Yu Zhuang¹, Aiguo Xing¹, Perry Bartelt², Muhammad Bilal¹, Zhaowei Ding³

4 ¹State Key Laboratory of Ocean Engineering, Shanghai Jiao Tong University, Shanghai, 200240, PR China

5 ²WSL Institute for Snow and Avalanche Research SLF, Flüelastrasse 11, 7260 Davos Dorf, Switzerland

6 ³State Key Laboratory of Geohazard Prevention and Geoenvironment Protection, Chengdu University of

7 Technology, Chengdu, 610059, China

8 **Correspondence:** Aiguo Xing (xingaiguo@sjtu.edu.cn)

9

10 **Abstract**

11 Landslides have been known to generate powerful air blasts capable of causing destruction and casualties

12 far beyond the runout of sliding mass. The extent of tree damage provides valuable information on air

13 blast intensity and impact region. However, little attention has been paid to the air blast-tree interaction.

14 In this study, we proposed a framework to assess the tree destruction caused by powerful air blasts,

15 including the eigenfrequency prediction method, tree motion equations and the breakage conditions. The

16 tree is modeled as a flexible beam with variable cross-sections, and the anchorage stiffness is introduced

17 to describe the tilt of tree base. Large tree deformation is regarded when calculating the air blast loading,

18 and two failure modes (bending and overturning) and the associated failure criteria are defined. Modeling

19 results indicate that although the anchorage properties are of importance to the tree eigenfrequency, tree

20 eigenfrequency is always close to the air blast frequency, causing a dynamic magnification effect for the

21 tree deformation. This magnification effect is significant in the cases with a low air blast velocity, while

22 the large tree deformation caused by strong air blast loading would weaken this effect. Furthermore,



23 failure modes of a specific forest subject to a powerful air blast depend heavily on the trunk bending
24 strength and anchorage characteristics. The large variation of biometric and mechanical properties of
25 trees necessitates the establishment of a regional database of tree parameters. Our work and the proposed
26 method are expected to make people better understand the air blast power and be of great utility for air
27 blast risk assessment in mountainous regions worldwide.

28 **Keywords:** Landslide-induced air blast; Tree eigenfrequency; Dynamic response; Tree breakage

29

30 **1 Introduction**

31 Long runout landslides involve massive amounts of energy and can be extremely hazardous owing to
32 their long movement distance, high mobility and potential chain disasters (Johnson and Campbell, 2017;
33 Shugar et al., 2021). A moving landslide with high velocity can generate a powerful air blast capable of
34 uprooting trees, lifting people into the air and even flattening buildings (Adams, 1881; Penna et al., 2021).
35 In recent decades, destructive air blasts frequently occurred in the mountainous regions worldwide and
36 caused casualties and economic loss far beyond the landslide runout (e.g. Yin, 2014; Bartelt et al., 2016;
37 Kargel et al., 2016). Understanding their force of destruction is of great utility for landslide risk
38 assessment and disaster mitigation in high altitude regions.

39 Monitoring equipment has been confirmed to provide great performance in determining the dynamic
40 characteristics of landslide-induced air blasts (Grigoryan et al., 1982; Sukhanov, 1982; Caviezel et al.,
41 2021). However, most case histories occurred in the high-altitude mountainous region without witnesses
42 (Yin and Xing, 2012), and the in-situ equipment can also get damaged because of the near-field
43 destruction of landslides and associated air blasts. Therefore, very few air blast cases were measured in
44 history. Geologists can only evaluate the air blast hazard for most recorded events using historical



45 evidence after the landslide occurred. In-situ information about forest destruction and tree breakage is
46 often used for the air blast risk assessment (Feistl et al., 2015; Fujita et al., 2017; Zhuang et al., 2019)
47 (Fig. 1). Uprooted trees and snapped stems delineate the impact region of air blasts and create a natural
48 vector field indicating the primary movement direction of the landslide, greatly helping analyze the
49 disaster-causing process of the event. In many cases, observations of forest destruction are the only data
50 to quantify air blast danger.



51

52 **Fig. 1** Trees breakage caused by the Wenjia valley landslide-induced air blast in Sichuan, China, 2008.

53 A question remained for air blast mitigation planning using the information of tree damage is how
54 to establish a simple relationship between air blast impact pressure and tree failure. Bending and
55 overturning are two common tree failure modes caused by strong winds. Trees snap when the bending
56 stress exerted by the air blast exceeds the wood strength (Peltola et al., 1999; Gardiner et al., 2000), while
57 the overturning will occur if the applied moment overcomes the anchorage resistance of root systems
58 (Jonsson et al., 2006; Nicoll et al., 2006). The occurrence of these two failure modes depends heavily on
59 both the air blast loading and tree properties. Considering the minor destruction of air blasts relative to



60 the landslide, although long recognized that sliding mass can easily break or uproot trees (Bartelt and
61 Stöckli, 2001; Šilhán, 2020), little attention has been paid to the tree destruction resulting from air blasts.
62 Furthermore, existing models describing the tree-air blast interaction are mostly static (Feistl et al., 2015)
63 or established based on the small-deformation theory (Bartelt et al., 2018). These methods could aid in a
64 rapid assessment of air blast power, but further research is needed to establish a dynamic model to
65 represent the dynamic response of trees in a strong wind. A mechanical understanding of how trees are
66 damaged by air blasts is therefore essential for quantifying the air blast powers and providing valuable
67 data to verify the possible numerical results.

68 In this study, we established a simple dynamic model capable of calculating the natural frequency
69 of trees and simulating their dynamic response subject to a powerful air blast. The proposed model
70 regards the tree as a multi-degree-of-freedom beam with variable diameters, and accounts for large tree
71 deflections and impacts of root anchorage. Both bending and overturning failure modes are involved in
72 the model. The work conducted in this study is expected to make people better understand the power of
73 landslide-induced air blasts and provide an applicable method to assess the air blast hazard.

74

75 **2. Model description**

76 Air blasts triggered by long runout landslides are characterized by high velocity and large impact regions,
77 which can cause forest destruction far beyond the landslide runout. Measurements of historical events
78 indicated that the air blast is intermittent and of short duration, lasting only a few seconds and could
79 reach a high velocity (Grigoryan et al., 1982; Sukhanov, 1982; Caviezel et al., 2021). This impulse wave
80 has a propagation distance of hundreds of meters in both horizontal and vertical directions, and acts over
81 the entire tree. Thus, the impact of air blasts on trees is similar to extreme wind gusts, producing large



82 bending moments in the stem and root base system, forcing trees to deform or get damage. Furthermore,
83 fallen trees often point to the movement direction of the landslide, illustrating there is little time for trees
84 to sway and react to air blasts while the inertial effects are greatly important.

85 To characterize the dynamic response of trees under the impact load of air blasts, we established a
86 mechanical model to predict the eigenfrequency of trees subject to air blasts and developed a dynamic
87 tree-swaying model that accounts for the large tree deformation. The tree is modeled as a flexible
88 cantilever beam with a variable cross-section. An anchorage stiffness of the root system is introduced to
89 represent the rotation at tree base. In what follows, we present the eigenfrequency prediction method,
90 tree motion equations and the breakage conditions.

91

92 *2.1 Eigenfrequency prediction*

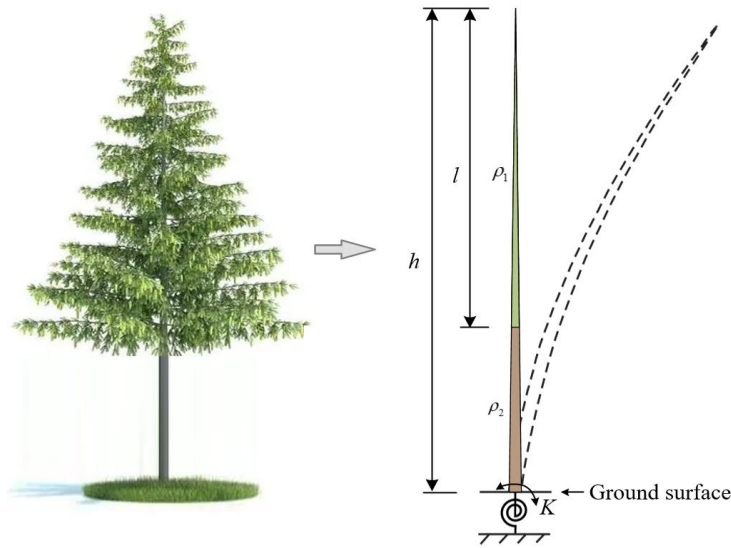
93 The tree is modeled as a flexible cantilever beam with variable diameters that is hinged at ground level
94 using elastic support. The beam diameter is assumed to continuous linearly decrease with height
95 regarding the decreasing diameters of trunk and crown from bottom to top, while the anchorage stiffness
96 of the root system (K) helps to describe the tilt of tree base in response to the moment (Neild and Wood,
97 1999). In the eigenfrequency prediction mode, the tree beam is divided into two segments with a splitting
98 point located at the starting point of the tree crown (Fig. 2). We assume that the tree crown shows minor
99 impacts on elastic modulus. The tree crown is accounted for through the crown mass, and thus the natural
100 difference between the two segments is the material density.

101 The governing differential equation for the dynamic bending of a nonuniform Euler-Bernoulli beam
102 is (Keshmiri et al., 2018):

$$103 \quad \rho A(z) \frac{\partial^2 u}{\partial t^2} + \frac{\partial^2 u}{\partial z^2} \left[EI(z) \frac{\partial^2 u}{\partial z^2} \right] = 0 \quad (1)$$



104 where z is the position variable along the beam length. For ease of calculation, the original point ($z=0$) is
 105 set at the treetop and the maximum value of z is at the tree base, so that the beam diameter $d(z)$
 106 corresponding to the position z can be described using a gradient coefficient (μ): $d(z)=\mu z$. u is the beam
 107 displacement, E is the elastic modulus, $A(z) = \frac{\pi}{4}(dz)^2$ and $I(z) = \frac{\pi}{64}(dz)^4$ are the cross-sectional area
 108 and moment of inertia, respectively.



109

110 **Fig. 2** Schematic representation of the eigenfrequency prediction model.

111 Plugging the expression of $A(z)$ and $I(z)$ into Eq. 1 gives:

$$112 \quad z^2 \frac{\partial^4 u}{\partial z^4} + 8z \frac{\partial^3 u}{\partial z^3} + 12 \frac{\partial^2 u}{\partial z^2} - \frac{16\rho\omega^2 u}{E\mu^2} = 0 \quad (2)$$

113 where ω is known as the eigenfrequency of the beam. The general solution of Eq. 2 can be expressed as:

$$114 \quad u(z) = \frac{1}{z} \left[A_1 J_2(2\sqrt{\lambda z}) + A_2 Y_2(2\sqrt{\lambda z}) + A_3 J_2(2i\sqrt{\lambda z}) + A_4 Y_2(2i\sqrt{\lambda z}) \right] \quad (3)$$

115 where $\lambda = \sqrt{\frac{16\rho\omega^2}{E\mu^2}}$, J_2 and Y_2 are the Bessel functions of the first and second kind (Mocica, 1988),

116 respectively, and A_1 - A_4 are coefficients that need to be determined based on the boundary conditions.

117 The deformation of the upper segment (crown) and the lower segment (trunk) can be generated in



118 a similar manner:

$$119 \quad u_1(z) = \frac{1}{z} \left[A_1 J_2(2\sqrt{\lambda_1 z}) + A_2 Y_2(2\sqrt{\lambda_1 z}) + A_3 J_2(2i\sqrt{\lambda_1 z}) + A_4 Y_2(2i\sqrt{\lambda_1 z}) \right] \quad 0 \leq z < l \quad (4)$$

$$120 \quad u_2(z) = \frac{1}{z} \left[B_1 J_2(2\sqrt{\lambda_2 z}) + B_2 Y_2(2\sqrt{\lambda_2 z}) + B_3 J_2(2i\sqrt{\lambda_2 z}) + B_4 Y_2(2i\sqrt{\lambda_2 z}) \right] \quad l \leq z \leq h \quad (5)$$

121 where l is the length of crown, h is the tree height, $\lambda_1 = \sqrt{\frac{16\rho_1\omega^2}{E\mu^2}}$ and $\lambda_2 = \sqrt{\frac{16\rho_2\omega^2}{E\mu^2}}$ are the single-valued

122 function of eigenfrequency. ρ_2 is the wood density and ρ_1 is the equivalent density regarding the

123 contribution of both tree trunk and crown. The boundary condition at the origin ($z=0$) is the free end, and

124 thus Eq. 4 can be simplified as:

$$125 \quad u_1(z) = \frac{1}{z} \left[A_1 J_2(2\sqrt{\lambda_1 z}) + A_3 J_2(2i\sqrt{\lambda_1 z}) \right] \quad 0 \leq z < l \quad (6)$$

126 According to continuity conditions of two segments at the splitting point and the boundary condition

127 at the tree base, following constraints are determined: $u_1(l) = u_2(l)$, $u_1'(l) = u_2'(l)$, $u_1''(l) = u_2''(l)$,

128 $u_1'''(l) = u_2'''(l)$, $u_2(h) = 0$, and $Ku_2'(h) + EI(h)u_2''(h) = 0$. Introducing the constraints into Eqs. (5-6), and

129 then the equations can be rewritten as:

$$130 \quad [F(\lambda_1, \lambda_2)]_{6 \times 6} \cdot [A_1 \quad A_3 \quad B_1 \quad B_2 \quad B_3 \quad B_4]^T \quad (7)$$

131 The orders of eigenfrequency and the corresponding vibration mode can be obtained by solving the

132 equation: the determinant of matrix $|F| = 0$.

133

134 2.2 Tree motion

135 The mechanical response of trees subject to an air blast is modeled using a modified multi-degree-of-

136 freedom tree swaying model with variable cross-sections (Zhuang et al., 2022). Different from the

137 simplification in the eigenfrequency prediction method, the size of tree crown here is determined based

138 on real tree data, corresponding to the frontal area distribution of the tree crown (Fig. 3(a)). The impact

139 of anchorage stiffness is involved in the vibration mode and eigenfrequency. The model divides the tree



140 beam into a set of segments and calculates the tree motion using linear modal analysis. Specifically, the
141 tree deformation is deposited into a set of vibration modes so that the total displacement is the combined
142 contribution of each mode. According to preliminary research performed by Sellier et al. (2008) and
143 Pivato et al. (2014), the contribution of the first vibration model is far ahead of the other modes for the
144 trees with a slender shape. Thus, only the first vibration mode and the corresponding eigenfrequency are
145 utilized in this study. The modeling of air blast pressure accounts for the wind-tree relative motion and
146 large tree deformations by regarding the beam velocity and geometric nonlinearities resulting from the
147 inclination of beam segments relative to the wind direction (θ_i) (Fig. 3(b)). With respect to the large tree
148 deformation, we also introduce the impact of eccentric gravity into the model, which contributes a lot
149 during the interaction with a powerful air blast. The gravity and wind load acting on each segment can
150 be easily calculated based on the predetermined diameter and frontal area distribution (Fig. 3(a)).
151 Considering that trees often fall in the direction of landslide motion and have little time to sway, the
152 maximum response of the tree is assumed to be reached before the damping forces act (Bartelt et al.,
153 2018). Only the undamped response to a short duration blast is considered. The tree motion equations
154 and the expression of air blast force are as follows:

$$155 \quad m \frac{\partial^2 y}{\partial t^2} + ky = \int_0^h F_i \phi ds + \int_0^h G_i \phi ds \quad (8)$$

$$156 \quad F_i = 0.5 \rho C_d A_f \left| v \cos \theta_i - \frac{\partial y}{\partial t} \cos \theta_i \right| \left(v \cos \theta_i - \frac{\partial y}{\partial t} \cos \theta_i \right) \cos \theta_i \quad (9)$$

$$157 \quad G_i = m_i g \cdot \sin \theta_i \cdot \cos \theta_i \quad (10)$$

158 where ϕ , w , $m = \int_0^h \bar{m} \phi^2 ds$, $k = 4\pi^2 m \omega^2$ are the first mode shape, the first eigenfrequency, modal mass
159 and stiffness, respectively, \bar{m} is the mass distribution, y is the associated generalized displacement, F_i
160 and G_i are the air blast loading and eccentric beam gravity act on the i th segment, h is the tree height, C_d
161 is the drag efficient, A_f is the frontal area, ρ and v are the density and velocity of the air blast, respectively.



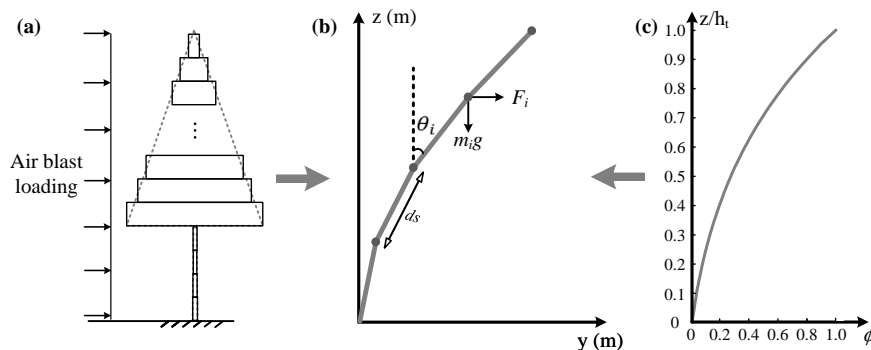
162 Our model is applicable of calculating the scenarios for both full-height and part-height air blasts.

163 In this study, the air blast velocity is expressed as a sine wave impulse with a short duration time t_0 :

164
$$v = v_{\max} \sqrt{\sin \varpi t} \tag{11}$$

165 where v_{\max} is the maximum velocity of the landslide-induced air blast and ϖ can be regarded as the
 166 circular frequency of the wind force $\varpi = \pi / t_0$ (wind force is related to the square of its velocity).

167 The mechanical response of trees subject to an air blast is deduced by introducing the calculated
 168 wind velocity from Eq. 11 into the tree motion model (Eqs. 8-9), and subsequently solving the equations
 169 using the central finite-difference scheme. The validity of this tree motion model has been checked by
 170 Pivato et al. (2014) and Zhuang et al. (2022), and thus the validation process is not involved here.



171 **Fig. 3** a-b Modeling the tree as a multi-degree-of-freedom flexible beam to calculate the dynamic
 172 response of trees submitted a powerful air blast. c The first mode shape of the beam helps to model the
 173 tree deformation.
 174

175 **2.3 Tree breakage**

176 Two failure modes commonly caused by air blasts are involved in the work: bending and overturning
 177 (Gardiner et al., 2000).

178 For the case of tree bending, trees are considered to break when the maximum bending stress σ_{\max}
 179 exceeds a critical value σ_{crit} :

180
$$\sigma_{\max} = \left[\frac{M(t, z) \cdot d(z) / 2}{I(z)} \right]_{\max} \geq \sigma_{\text{crit}} \tag{12}$$



181 where σ_{crit} is the bending strength of the tree, which depends highly on the material property. $M(t, z)$ is
 182 the bending moment, and its value is calculated at each time step all along the beam:

$$183 \quad M(t, z) = EI(z) \frac{d\theta}{ds} \quad (13)$$

184 where $\frac{d\theta}{ds}$ represents the local beam curvature and θ is the angle between the beam segment with the
 185 vertical direction.

186 For the tree overturning case, trees are regarded to break at the basement when the air blast-induced
 187 moment reaches the anchorage resistance (M_{crit}):

$$188 \quad M_{base}(t) \geq M_{crit} \quad (14)$$

189 where $M_{base}(t)$ is the moment at tree base calculated at each time step, and the anchorage resistance M_{crit}
 190 is often determined based on in-situ tests (e.g. tree pulling tests).

191

192 3. Application

193 To demonstrate the power of air blasts and how they damage trees, we consider the problem proposed
 194 by Bartelt et al. (2018): a landslide-induced air blast enters a spruce forest at high speed (maximum
 195 velocity of 20 m/s). The short-duration air blast lasts a few seconds with a frequency ω . Trees in the
 196 forest have a height between 25 and 30 m, which is also the height of the air blast. The sliding mass has
 197 stopped before reaching the forest and only the air blast loads on the trees.

198 **Table 1** Model parameters used in the numerical simulations of the tree response. Parameters are derived
 199 from data contained in Kantola and Mäkelä (2004) and Bartelt et al. (2018).

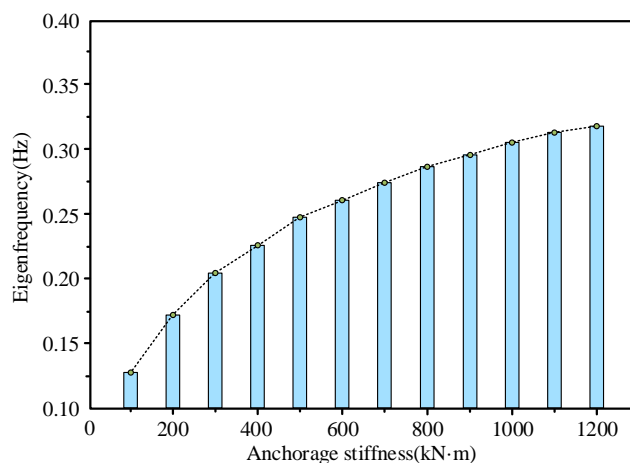
Height h (m)	Crown height l (m)	Crown width w (m)	Diameter at trunk base D (m)	Wood density ρ_2 (kg/m ³)	Branch mass m (kg)	Drag coefficient C_d
27	18	5	0.4	480	540	0.4

200 Using the measured biomass parameters presented in Table 1, we set the total crown mass of a single
 201 tree to be 540 kg. The tree crown is assumed to be a cone with a length of 18 m ($\frac{2}{3}h$) and a width of 5



202 m. The wood density is 480 kg/m^3 and the elastic modulus is 10 GPa. Measurements of root anchorage
203 stiffness (K) are very rare and in-situ tests on spruce performed by Neild and Wood (1999) show a value
204 variation of 80-1200 $\text{kN}\cdot\text{m}$. This value range indicates a large variation in K depending on the growth
205 conditions, and the values of 100-1200 $\text{kN}\cdot\text{m}$ are applied in the prediction of eigenfrequency and
206 vibration mode in this study.

207 The eigenfrequency ranging from 0.13 Hz ($K=100 \text{ kN}\cdot\text{m}$) to 0.32 Hz ($K=1200 \text{ kN}\cdot\text{m}$) is calculated
208 based on the above parameters (Fig. 4). The modeled results are in high agreement with measurements
209 performed by Jonsson et al. (2007) (0.16-0.30 Hz), indicating the validity of our proposed eigenfrequency
210 prediction method. Although the tree eigenfrequency varies significantly with the anchorage stiffness, all
211 the calculated values are less than 0.5 Hz. The same order of magnitude between tree eigenfrequency
212 and air blast frequency necessitates a further investigation on the possible impact of resonance. The
213 dynamic magnification effect caused by impulse loading can greatly amplify the static stress state,
214 making the trees easier to be damaged.



215
216 **Fig. 4** Eigenfrequency of trees corresponding to different anchorage stiffness.

217 To investigate the impact of dynamic magnification, we performed simulations for all the scenarios
218 using the tree eigenfrequency of 0.26 Hz ($K=600 \text{ kN}\cdot\text{m}$) and the associated vibration mode. A



219 magnification factor D is defined to describe this effect:

$$220 \quad D = \frac{u_{d,max}(\beta)}{u_{sta}} = \frac{u_{d,max}(\beta)}{\int_0^h F_{s,max} \phi ds / k} = \frac{u_{d,max}(\beta)}{\int_0^h \rho C_d A_f v_{max}^2 \phi ds / k} \quad (15)$$

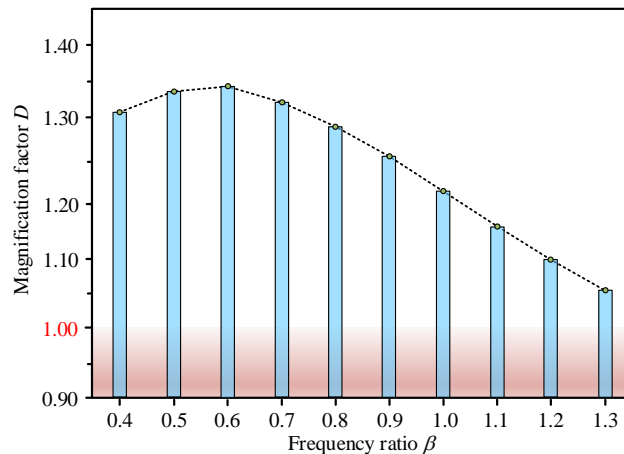
221 where $u_{d,max}$ and u_{sta} are the maximum deformation subject to dynamic load and static load, respectively,

222 $F_{s,max}$ is the static wind force corresponding to the maximum air blast velocity and $\beta = \frac{\varpi}{\omega}$ is the ratio

223 between the air blast frequency (ϖ) and the eigenfrequency of the tree (ω). Notably, the air blast is a

224 multi-medium fluid that contains numerous dusts and $\rho = 5\text{ kg/m}^3$ is utilized here (Feistl et al., 2015). In

225 this scenario u_{sta} is calculated to be 9.8 m.



226

227 **Fig. 5** Magnification factor with various frequency ratio.

228 Fig. 5 shows the impact of air blast frequency on the dynamic magnification effect. A parabola

229 relationship is identified between the magnification factor and the frequency ratio. Consider first an

230 impulse air blast lasting 1.6 s ($\beta = 1.2$). The air blast frequency is higher than that of the tree, implying

231 the maximum deformation reaches after the loading time. The modeled maximum dynamic deformation

232 $u_{d,max}$ reaches 10.7 m, and the magnification factor is 1.09. In this case, the magnification effect of tree

233 deformation seems not significant because of the large tree deformation and short-duration loading, and

234 the modeled result is similar to the static stress state. For a longer air blast duration of 3.2 s ($\beta = 0.6$), we



235 find $D=1.34$, a high value. The maximum tree deformation reaches during the air blast loading. In such
236 a scenario, an air blast travelling at 20 m/s can exert similar destruction as a long-duration wind moves
237 at 25 m/s. The dynamic magnification effect significantly increases the tree deformation and thus causes
238 such a phenomenon. Measurements of air blast duration reported by Russian and Swiss researchers
239 (Grigoryan et al., 1982; Sukhanov, 1982) are within this range, lasting only a few seconds. The main
240 finding drawn from the analysis is that the air blast frequency is close to the tree eigenfrequency.
241 Although the large tree deformation decreases the wind loading, the impulse air blast load is prone to
242 damage the trees because of the dynamic magnification effect.

243 Additional simulations were performed on the air blast induced-tree breakage. The impulse air blast
244 is assumed to have a maximum velocity of 20 m/s and a duration of 3.2 s. For this case, numerical results
245 demonstrate the maximum bending stress and moment of 35 Mpa and 192 kN·m, respectively. The
246 maximum bending stress reaches at 9 m height ($1/3h$), and the maximum bending moment is identified
247 at the tree base. In natural forest areas, the bending strength σ_{crit} and anchorage resistance M_{crit} are highly
248 variable, depending on tree species, soil characteristics and temperatures, etc. Measurements conducted
249 by Peltola et al. (2000) and Lundström et al. (2007) indicate that the bending stress to destroy mature
250 trees needs to exceed a value of 30 MPa while mature spruces with a height of 20-40 m have an anchorage
251 resistance reaches up to 100-400 kN·m. For the case performed in this study, the forest is likely to damage
252 in both bending and overturning failure modes. Reliable values of critical parameters are needed during
253 the assessment of tree destruction, and this will improve the prediction accuracy of the likely failure
254 mode.

255

256



257 **4. Discussion**

258 Risk assessment and disaster mitigation of landslide-induced air blasts are hot issues in mountainous
 259 regions. Developing a simple but applicable relationship between air blast pressure and tree failure is of
 260 great utility for scientists to quantify the air blast power. Compared with existing models, one significant
 261 improvement of our model is to model the tree as a flexible beam with variable cross-section and involve
 262 the impact of anchorage. This improvement allows the tree to move as its natural vibration mode rather
 263 than a hypothetical trajectory (e.g. rotate around the tree base as a rigid body (Bartelt et al., 2018)).
 264 Moreover, the variable cross-section makes the modeling of tree bending failures more realistic. We can
 265 simulate the failure position of trees subjected to a powerful air blast. For the existing model with a
 266 constant diameter (Feistl et al., 2015), the rigidity EI is constant along the beam, and the maximum
 267 bending stress is always identified at the tree base. This failure characteristic cannot match the actual
 268 situation well.

269 Our proposed model further accounts for the impacts of large tree deformation: eccentric gravity
 270 and modeling of air blast force regarding the wind-tree relative motion and geometric nonlinearities.
 271 These factors are of great importance when the tree is subjected to a powerful air blast. To investigate
 272 the impact of these factors, we conducted a comparative analysis by simplifying the tree motion model
 273 of Eq. 8 without involving the impact of large tree deformation. The simplified model is similar to that
 274 proposed by Bartelt et al. (2018):

275
$$m \frac{\partial^2 y}{\partial t^2} + ky = \int_0^h 0.5 \rho C_d A_f v_{\max}^2 \phi ds \cdot \sin \varpi t = \int_0^h F_{s, \max} \phi ds \cdot \sin \varpi t \quad (16)$$

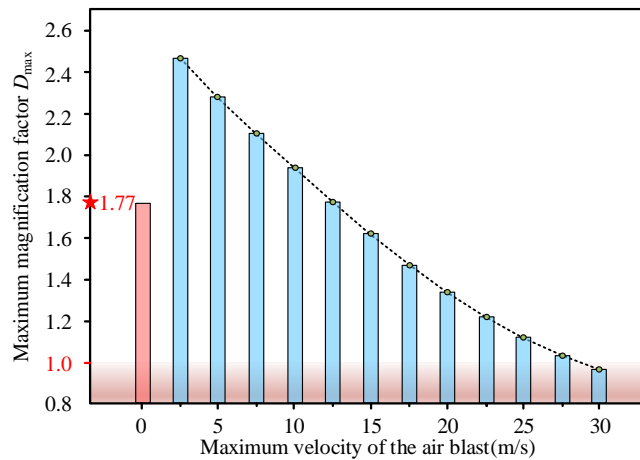
276 The deformation at the tree top can be written as:

277
$$\begin{cases} x(t) = \frac{\int_0^h F_{s, \max} \phi ds}{k} \frac{1}{1 - \beta^2} (\sin \varpi t - \beta \sin \omega t) & 0 \leq t \leq t_0 \\ x(t) = \frac{x'(t_0)}{\omega} \sin \omega(t - t_0) + x(t_0) \cos \omega(t - t_0) & t > t_0 \end{cases} \quad (17)$$



278 The maximum deformation occurs during the loading time when $\beta \leq 1$, and after the loading
 279 time when $\beta > 1$. The magnification factor D for both scenarios can be expressed as:

$$280 \quad \begin{cases} D = \frac{1}{1-\beta^2} \left[\sin\left(\frac{2\pi\beta}{\beta+1}\right) - \beta \sin\left(\frac{2\pi}{\beta+1}\right) \right] & \beta \leq 1 \\ D = \frac{2\beta}{\beta^2-1} \cos\left(\frac{\pi}{2\beta}\right) & \beta > 1 \end{cases} \quad (18)$$



281
 282 **Fig. 6** Impact of large tree deformation on the maximum magnification factor D_{max} . The red star
 283 represents the D_{max} calculated from Eq. 18. The red bar represents the D_{max} corresponding to the scenario
 284 with a very low air blast velocity (maximum velocity of 0.1m/s) and the eccentric gravity is not
 285 considered.

286 Fig. 6 presents the impact of large tree deformation on the magnification effect. We first perform
 287 the simulation using the proposed model without regarding the impact of large tree deformation. A very
 288 low air blast velocity (maximum velocity of 0.1m/s) is performed and the eccentric gravity is not
 289 considered. The D_{max} value of 1.77 is identified in the scenario, which is consistent with the analytical
 290 solution from Eq. 18. The tree deformation is small with such a weak air blast loading, and the
 291 comparison result verifies the validity of our proposed model. Further calculations with higher air blast
 292 velocities show different results. In the cases of a low air blast velocity, the eccentric gravity contributes
 293 a lot to the tree deformation, causing a rather large magnification factor (>2). However, D_{max} greatly
 294 decreases with the increase of wind velocity. For a high air blast velocity, the dynamic response and



295 eccentric gravity amplify the tree deformation, but the inclination of the trees to the wind direction
296 significantly reduces the air blast loading. This special mechanism was rarely considered during the
297 previous assessment of landslide-induced air blasts. We suggest that the modeled tree deformation
298 subjected to a powerful air blast might be overestimated without considering large tree deformation,
299 although this simplified model of Eq. 18 has the advantage of rapid assessment for air blast pressure. The
300 impact of large tree deformation should be accounted for when using forest destruction to quantify the
301 air blast danger.

302 The dynamic response of trees subject to a landslide-induced air blast is a complex problem,
303 depending heavily on the biometric characteristics of trees. Some biomass variations can be represented
304 by the parameters in the proposed model. For example, for the leafless trees, air blasts pass through the
305 tree crown and only act on the branches, causing a smaller wind load. A reduction of drag efficient C_d is
306 needed in such a condition. Single trees in the impact region of air blasts are subject to a larger loading
307 than trees in dense forest stands, where tree crowns tend to be narrower and form a shielding effect. We
308 can make a reduction in the frontal area A_f to simulate this mechanism. Furthermore, although much
309 effort has been paid to the biometric and mechanical characteristics of tree crowns and trunks, less
310 information is available about the anchorage stiffness and resistance. The root anchorage properties
311 significantly influence the tree eigenfrequency and the likely failure mode. A reliable measurement value
312 of tree bending strength and anchorage resistance is of utility to improve the accuracy of tree failure
313 prediction and clarify which failure mode is prone to occur. Overall, biomass-related parameters selected
314 to estimate the air blast pressure are recommended to be determined based on in-situ investigations. In
315 the future, more measurements need to be conducted on the anchorage properties of trees. Regional
316 databases for biometric and mechanical properties of trees are worthwhile to be established. This would



317 help provide reliable parameters for the air blast risk assessment.

318 In this study, the tree is modeled as a variable cross-section that is hinged at ground level using
319 elastic support. Root anchorage is complex and sensitive to many factors such as soil mechanical
320 properties, soil water content and root morphology, and we acknowledge that it is difficult to establish a
321 model that accounts for all the factors that affect the anchorage. Most importantly, we developed a simple
322 but practical model that could simulate the dynamic response of trees subject to a powerful air blast and
323 their two possible failure modes. Bartelt and his colleagues (Bartelt et al., 2018) have developed a
324 dynamic model named RAMMS, which could efficiently model the entire movement process of
325 ice/rock/snow avalanches and the associated air blasts. It is anticipated that the combination of our
326 proposed tree model and the RAMMS dynamic model could help the risk assessment of potential air
327 blasts through modeling the air blast impact region and forest destruction.

328

329 **Conclusions**

330 Air blasts are short-duration impulses and can intensify the potential destruction far beyond the sliding
331 mass. Trees destruction in-situ can provide valuable data to quantify the air blast danger and make us
332 better understand its force of destruction. In this study, we developed a framework for the forest
333 destruction assessment subject to a powerful air blast, including the eigenfrequency prediction method,
334 tree motion equations and breakage conditions. The tree is modeled as a flexible variable cross-section
335 beam hinged at ground using elastic support. The impacts of root anchorage and large tree deformation
336 are regarded during the dynamic response analysis. The framework also involved two failure modes
337 (bending and overturning) and the corresponding failure criteria so that the risk of forest damage could
338 be assessed.



339 Using the proposed framework, we assumed conditions to investigate the air blast power. Modeling
340 results demonstrate that although the anchorage properties significantly influence the tree eigenfrequency,
341 the tree eigenfrequency is always in the same order as air blast frequency. The associated dynamic
342 magnification effect amplifies the tree deformation and thus makes the tree damage easier. In the scenario
343 with a similar frequency between air blasts and trees, an air blast travelling at 20 m/s causes a similar
344 force of destruction as a long-duration wind load moves at 25 m/s. Notably, this magnification effect
345 caused by the dynamic response and eccentric gravity is significant in the cases of low wind velocity,
346 while the large tree deformation caused by strong air blast loading would weaken this effect. Furthermore,
347 bending and overturning are two likely failure modes for trees subject to a powerful air blast, but exactly
348 what kind of failure will occur for a specific forest depends heavily on the properties of both trees and
349 soil. In the future, more measurements should be conducted on biometric and mechanical properties of
350 trees, and a regional parameter database is worthwhile to be established. This would greatly improve the
351 prediction accuracy of tree damage and air blast pressure. The work conducted in this study is expected
352 to make people better understand the air blast power and provide an applicable method for the risk
353 assessment of landslide-induced air blasts.

354

355 **Data availability**

356 No data sets were used in this article.

357

358 **Author contribution**

359 Yu Zhuang did the numerical work and wrote the manuscript with contributions from all co-authors.

360 Aiguo Xing and Perry Bartelt designed the work and modified the manuscript. Bilal Muhammad



361 evaluated the results and proposed various improvements that were incorporated. Zhaowei Ding helped
362 with the eigenfrequency prediction model.

363

364 **Competing interest**

365 The authors declare that they have no known competing financial interests or personal relationships that
366 could have appeared to influence the work reported in this paper.

367

368 **Acknowledgments**

369 This study was supported by the National Natural Science Foundation of China (No. 41977215).

370

371 **References**

372 Adams, J.: Earthquake-dammed lakes in New Zealand, *Geology*, 9, 215-219, 1881.

373 Bartelt, P., and Stöckli, V.: The influence of tree and branch fracture, overturning and debris entrainment
374 on snow avalanche flow, *Annals of Glaciology*, 32, 209-216, 2001.

375 Bartelt, P., Buser, O., Vera Valero, C., and Bühler, Y.: Configurational energy and the formation of mixed
376 flowing/powder snow and ice avalanches, *Annals of Glaciology*, 57(71), 179-188, 2016.

377 Bartelt, P., Bebi, P., Feistl, T., Buser, O., and Caviezel, A.: Dynamic magnification factors for tree blow-
378 down by powder snow avalanche air blasts, *Natural Hazards Earth System Sciences*, 18, 759-764,
379 2018.

380 Bartelt, P., Christen, M., Bühler, Y., and Buser, O.: Thermomechanical modelling of rock avalanches with
381 debris, ice and snow entrainment, *Numerical Methods in Geotechnical Engineering IX*, Taylor &
382 Francis Group, London, pp 1047-1054, 2018.



- 383 Caviezel, A., Margreth, S., Ivanova, K., Sovilla, B., and Bartelt, P.: Powder snow impact of tall vibrating
384 structures, *Eccomas Proceedia Compdyn*, 5318-5330, 2021.
- 385 Feistl, T., Bebi, P., Christen, M., Margreth, S., Diefenbach, L., and Bartelt, P.: Forest damage and snow
386 avalanche flow regime, *Natural Hazards and Earth System Sciences*, 15, 1275-1288, 2015.
- 387 Fujita, K., Inoue, H., Izumi, T., Yamaguchi, S., Sadakane, A., Sunako, S., Nishimura, K., Immerzeel, W.
388 W., Shea, J. M., Kayastha, R. B., Sawagaki, T., Breashears, D. F., Yagi, H., and Sakai, A.:
389 Anomalous winter-snow-amplified earthquake-induced disaster of the 2015 Langtang avalanche in
390 Nepal, *Natural Hazards Earth System Sciences*, 17, 749-764, 2017.
- 391 Gardiner, B., Peltola, H., and Kellomäki, S.: Comparison of two models for predicting the critical wind
392 speeds required to damage coniferous trees, *Ecological Modelling*, 129, 1-23, 2000.
- 393 Grigoryan, S., Urubayev, N., and Nekrasov, I.: Experimental investigation of an avalanche air blast, *Data*
394 *Glaciology Student*, 44, 87-93, 1982.
- 395 Jonsson, M. J., Foetzki, A., Kalberer, M., Lundström, T., Ammann, W., and Stöckli, V.: Root-soil rotation
396 stiffness of norway spruce (*Picea abies* (L.) Karst) growing on subalpine forested slopes, *Plant Soil*,
397 285, 267-277, 2006.
- 398 Johnson, B. C., and Campbell, C. S.: Long-runout landslides are among the most spectacular and
399 catastrophic geologic processes, *Geophysical Research Letters*, 44(12), 12091-12097, 2017.
- 400 Kantola, A., and Mäkelä, A.: Crown development in Norway spruce [*Picea abies*(L.) Karst.], *Trees*, 18,
401 408-421, 2004.
- 402 Kargel JS, et al. (2016) Geomorphic and geologic controls of geohazards induced by Nepal's 2015
403 Gorkha earthquake. *Science*, 351, aac8353.
- 404 Keshmiri, A., Wu, N., and Wang, Q.: Free Vibration Analysis of a Nonlinearly Tapered Cone Beam by



- 405 Adomian Decomposition Method, *International Journal of Structural Stability and Dynamics*, 18(7),
406 1850101, 2018.
- 407 Lundström, T., Jonsson, M. J., and Kalberer, M. The root-soil system of Norway spruce subjected to
408 turning moment: resistance as a function of rotation, *Plant Soil*, 300, 35-49, 2007.
- 409 Mocica, G.: *Special Functions Problems*, Bucharest: Didactic and Pedagogic Publishing House, 1988.
- 410 Neild, A. S., and Wood, C. J.: Estimating stem and root-anchorage flexibility in trees, *Tree Physiology*,
411 19, 141-151, 1999.
- 412 Nicoll, B. C., Gardiner, B. A., Rayner, B., Peace, A. J.: Anchorage of coniferous trees in relation to
413 species, soil type, and rooting depth, *Canadian Journal of Forest Research*, 36, 1871-1883, 2006.
- 414 Penna, I. M., Hermanns, R. L., Nicolet, P., Morken, O. A., and Jaboyedoff, M.: Airblasts caused by large
415 slope collapses, *Geological Society of America Bulletin*, 133, 939-948, 2021.
- 416 Peltola, H., Kellomäki, S., Väisänen, H., and Ikonen, V.: A mechanistic model for assessing the risk of
417 wind and snow damage to single trees and stands of scots pine, norway spruce, and birch, *Canadian*
418 *Journal of Forest Research*, 29, 647-661, 1999.
- 419 Peltola, H., Kellomäki, S., Hassinen, A., and Granander, M.: Mechanical stability of Scots pine, Norway
420 spruce and birch: an analysis of tree-pulling experiments in Finland, *Forest Ecology and*
421 *Management*, 135, 143-153, 2000.
- 422 Pivato, D., Dupont, S., and Brunet, Y.: A simple tree swaying model for forest motion in windstorm
423 conditions, *Trees*, 28, 281-293, 2014.
- 424 Sellier, D., Brunet, Y., and Fourcaud, T.: A numerical model of tree aerodynamic response to a turbulent
425 airflow, *Forestry*, 81(3), 279-297, 2008.
- 426 Shugar, DH. et al.: A massive rock and ice avalanche caused the 2021 disaster at Chamoli, Indian



- 427 Himalaya, *Science*, 373(6552), 300-306, 2021.
- 428 Šilhán, K.: Tree ring evidence of slope movements preceding catastrophic landslides, *Landslides*, 17,
429 615-626, 2020.
- 430 Sukhanov, G.: The mechanism of avalanche air blast formation as derived from field measurements, *Data*
431 *Glaciology Student*, 44, 94-98, 1982.
- 432 Yin, Y. P., and Xing, A. G.: Aerodynamic modeling of the yigong gigantic rock slide-debris avalanche,
433 Tibet, China. *Bulletin of Engineering Geology and the Environment*, 71, 149-160, 2012.
- 434 Yin, Y. P.: Vertical acceleration effect on landslides triggered by the Wenchuan earthquake, China.
435 *Environmental Earth Sciences*, 71, 4703-4714, 2014.
- 436 Zhuang, Y., Xu, Q., and Xing, A. G.: Numerical investigation of the air blast generated by the Wenjia
437 valley rock avalanche in Mianzhu, Sichuan, China, *Landslides*, 16, 2499-2508, 2019.
- 438 Zhuang, Y., Xing, A. G., Jiang, Y. H., Sun, Q., Yan, J. K., and Zhang, Y. B.: Typhoon, rainfall and trees
439 jointly cause landslides in coastal regions, *Engineering Geology*, 298, 106561, 2022.